

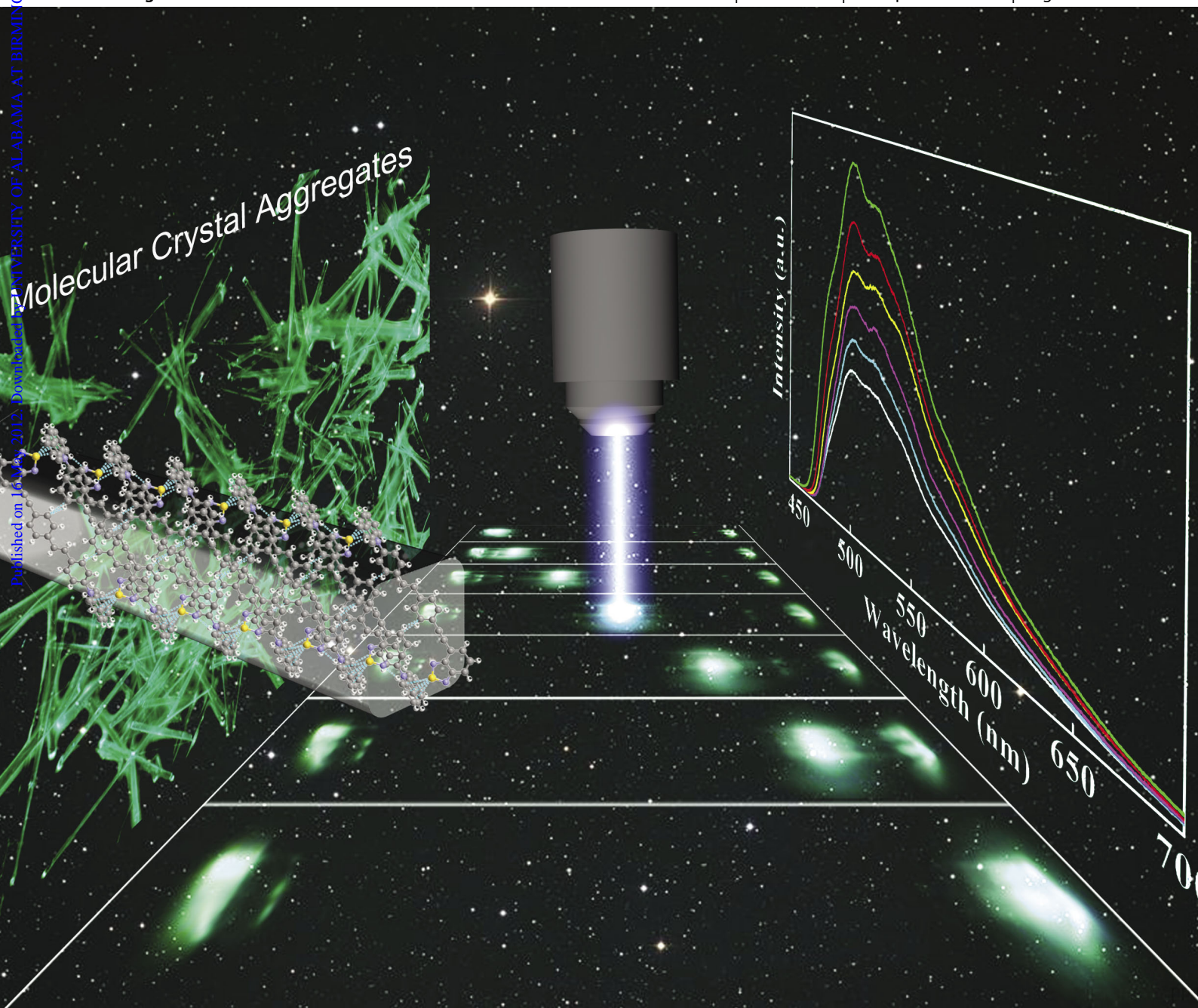
ChemComm

Chemical Communications

www.rsc.org/chemcomm

Volume 48 | Number 72 | 18 September 2012 | Pages 8981–9096

Published on 16 May 2012. Downloaded by UNIVERSITY OF ALABAMA AT BIRMINGHAM on 26/10/2014 06:48:37.



ISSN 1359-7345

RSC Publishing

COMMUNICATION

Yuliang Li *et al.*

Controlling growth of molecular crystal aggregates for efficient optical waveguides



1359-7345(2012)48:72;1-Y

Cite this: *Chem. Commun.*, 2012, **48**, 9011–9013

www.rsc.org/chemcomm

COMMUNICATION

Controlling growth of molecular crystal aggregates for efficient optical waveguides†

Songhua Chen,^a Nan Chen,^a Yong Li Yan,^b Taifeng Liu,^a Yanwen Yu,^a Yongjun Li,^a Huibiao Liu,^a Yong Sheng Zhao^b and Yuliang Li^{*a}

Received 7th April 2012, Accepted 16th May 2012

DOI: 10.1039/c2cc32501b

Controllable crystal aggregate structures which show highly uniform crystal tubule, rod and cubic like architectures were achieved and the well-defined microrods exhibit outstanding optical waveguide properties.

During the past decade, well-defined nano- and microstructured materials have been paid more and more attention for their potential applications in the electronics and photonics fields.^{1–3} They are also attractive as building blocks as their individual structures can function as both device elements and interconnects.⁴ Typically, during this phase of development of a new science and technology area, researchers focus mainly on understanding the nature of structure–function relationships. Intramolecular charge-transfer (ICT) molecules that exhibit multifunctionality such as multiple electroactivity or photoactivity offer wide applications in organic electronics, due to their semiconductor character and high charge carrier mobilities.⁵ ICT molecules in particular have potential in applications of photoelectric devices.⁶ The results are able to help reach the goal of physical measurement. In this communication, we have designed and synthesized donor–acceptor (D–A) molecules based on benzothiadiazole, where the donor part consists of carbazole units, while benzothiadiazole works as the acceptor. Supramolecular self-assembly processes offer considerable synthetic advantages for fine tuning the size, shape and distribution and exploiting the supramolecular interaction for controlling the growth of these ICT compounds in the form of microtubes, microrods and cubic structures in large quantities and with high morphological and chemical purity.

Single crystals of **BTN-6** were obtained by slow diffusion of n-hexane into tetrahydrofuran (THF) solution at room

temperature, while **BTN-7** crystals were grown by slow evaporation of CHCl_3 (Fig. 1).‡ Analysis of the crystal structure demonstrates that **BTN-6** has a nonplanar conformation and a twisted structure in the crystals. The angle between the carbazole unit and neighboring benzene ring is about 53.1° . While, two benzene rings linked by the acetylenic and ethylenic linkage bond are nearly coplanar with the benzothiadiazole unit, suggesting that an extended π -conjugated system exists in this part of the molecule. **BTN-6** has four molecules per unit cell with the molecules arranged into two non-equivalent stacks and with their dipoles pointing in opposite directions.⁷ One remarkable feature of the crystal structure is the existence of short $\text{S}_1 \cdots \text{N}_2$ interheteroatom contacts (3.09 \AA) between the two 1,2,5-thiadiazole rings and $\text{S}_1 \cdots \text{H-C}$ interactions (2.97 \AA) from the benzene ring, which also played an important role in the parallel creation of this packing structure (Fig. S1†). Furthermore, the presence of the terminal NO_2 group on benzothiadiazole in **BTN-6** gives rise to intermolecular aromatic hydrogen bonding: $\text{C-H} \cdots \text{O}$ (2.59 \AA) hydrogen bond, and the π - π interactions between the ethylenic bond and benzothiadiazole ring, which are also critical for the head-to-tail crystal packing. These hydrogen bonds extend over the whole crystal structure and the multiple intermolecular interactions help lock the molecular conformations.⁸ The stabilized conformations are resistant to intramolecular motion induced by thermal agitation. This kind of molecular configuration can effectively promote the π - π interaction in the solid state and may have caused the intense fluorescence in the aggregation state.⁹ When viewed down the crystallographic *b*-axis, the molecules are π -stacked (interplanar distance of 3.20 \AA) in two translational stacks.

BTN-7 shares some structural similarities with compound **BTN-6**, such as the perfect planarity of the benzothiadiazole acceptor and π -conjugated linkage. Hence, the π -orbital overlap between the rings of a single molecule is close to its maximum value.⁷ Whereas, the dihedral angle between the carbazole unit and neighboring benzene ring is 67.8° , slightly larger than the dihedral angle found in **BTN-6**. The closest approaches of a molecule in one stack to a molecule in an adjacent stack are as

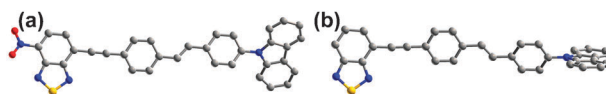


Fig. 1 Crystal structures of **BTN-6** (a) and **BTN-7** (b).

^a CAS Key Laboratory of Organic Solids, Beijing National Laboratory for Molecular Science (BNLMS), Institute of Chemistry, Chinese Academy of Sciences, Beijing, 100190, P. R. China. E-mail: ylli@iccas.ac.cn

^b CAS Key Laboratory of Photochemistry, Beijing National Laboratory for Molecular Science (BNLMS), Institute of Chemistry, Chinese Academy of Sciences, Beijing, 100190, P. R. China

† Electronic supplementary information (ESI) available: Synthetic details, UV-Vis and fluorescence spectra, AFM images. CCDC-859087 for **BTN-6** and CCDC-859088 for **BTN-7**. For ESI and crystallographic data in CIF or other electronic format see DOI: 10.1039/c2cc32501b

follows: $N_1 \cdots H-C$ (2.68 Å); $C-H \cdots \pi$ (2.69 Å) between adjacent carbazole rings. One remarkable feature of the crystal structure is the existence of $S_1 \cdots \pi$ (3.15 Å) contacts between the heteroatom and carbazole.

These compounds have a narrow peak at ~ 340 nm (Fig. S2†) attributable to the $\pi \rightarrow \pi^*$ transition of the benzothiadiazole unit,¹⁰ and a feature absorbance band indicating the intramolecular charge transfer from the carbazole group to the benzothiadiazole acceptor core.¹¹ The results showed the ICT band of 448 nm for **BTN-6** was longer than 384 nm for **BTN-7** due to the stronger electron accepting of the NO_2 group.¹² In this way, the position of the ICT band in the visible region could be modulated by using the different electron acceptor on the benzothiadiazole. **BTN-7** showed intense fluorescence in solution. While, no emission was detected for **BTN-6** in solution (CH_2Cl_2 , $CHCl_3$, THF, etc.). However, the nanostructure suspension or solid state of **BTN-6** was a good emitter. The fluorescence enhancement process was studied with different ratios of hexane/THF mixture. Hexane was continually added to the **BTN-6** solution in THF while keeping a total concentration of 2.0×10^{-5} M. The PL intensity remained almost unchanged when the content of hexane was lower than 40% and increased greatly when the hexane content was higher than 50%. Meanwhile, the emission peak showed a blue-shift on increasing the hexane (Fig. S3†). However, if the content of hexane was higher than 85%, the fluorescence intensity of the suspension gradually weakened instead of intensifying, because the mixed solvent becomes so poor that the molecular aggregates begin to precipitate in the solvents. The enhanced fluorescence emission of **BTN-6** is a typical aggregation-induced emission system.¹³

The crystal data showed that the **BTN-6** molecule is a sticky structure. Effective $\pi-\pi$ interactions, hydrogen bonding and a large dipole-dipole moment were observed in the solid state. The solubility of **BTN-6** was poor in conventional organic solvents such as methanol, acetonitrile, hexane, and toluene, etc. Slow crystallization was performed at the interface between a “good” and a “poor” solvent. Well-defined microtube structures of **BTN-6** were successfully fabricated by a phase transfer methodology.¹⁴ Hexane was used as a “poor” solvent, while THF was used as a “good” solvent in the system. After the addition of 90% volume fractions of hexane into the THF solution, 1-D microtubule structures were observed as precipitates in the mixture solution and stable even for 4 months (Fig. 2a). Atomic force microscopy images (Fig. S4†) showed the tubes have a smooth surface with a typical height and width of 500 nm and 3.0 μm , respectively.

The shape and size of the microstructures of **BTN-6** can be tuned by changing the “poor” solvent. As described above, large-scale 1-D microrods were observed as precipitates in ethanol/THF mixture solutions. The microrods were about 2–3 μm in width and 10–15 μm in length (Fig. 2c). However, when the saturated refluxing solution of **BTN-6** in THF was cooled to room temperature, the precipitates were observed to be “cubic” superstructure assemblies (Fig. 2e). Beyond the solution processing methods, a solvent-vapor annealing technique has been successfully used for self-assembly of **BTN-7** molecules on substrates. Well-defined 1-D microrods can be simply obtained by injection of a concentrated CH_2Cl_2

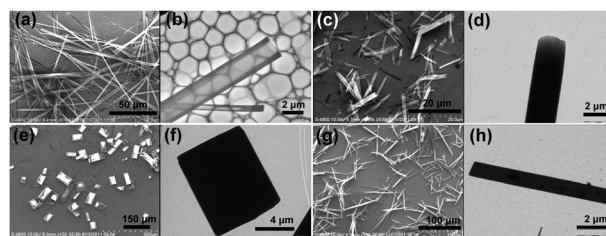


Fig. 2 Large-area SEM and TEM images of **BTN-6**: microtubes (a–b), microrods (c–d), microcrystals (e–f). Microrod structure of **BTN-7** (g–h).

solution into poor, same volume solvent hexane with sufficient stirring (Fig. 2g). **BTN-7**, with the predominant $\pi-\pi$ interaction, were rapidly dispersed from a “good” solvent into a “poor” solvent, where the molecules have limited solubility and thus self-assembly of these molecules was expected to occur instantaneously.¹⁵ This approach provides *in situ* preparation of microrods on a surface which is suitable for optical or microscopy investigation. By these simple solution methods, these ICT compounds were constructed as well-ordered and stable micro-sized suprastructures without any addition of surfactant, catalyst, or template.

X-Ray diffraction experiments (Fig. S5 and S6†) confirmed that these supramolecular self-assemblies were crystalline, according to the sharp diffraction peaks. In the case of **BTN-6**, there are distinct peaks corresponding to the (0 0 2), (1 0 -3) and (1 2 -4) planes in the microtube structures and (0 0 2), (0 2 2) and (1 2 -4) planes in the microrod structures, revealing that the molecules may tend to stack along the *c*-axis to form the 1-D structures. As described, the operation parameters such as temperature, concentration, and growth time remarkably affected the morphologies of the molecular crystals in different self-assembled systems, due to the interactions of hydrogen bonds and $\pi-\pi$ stacking in different chemical environments. The morphologies of the final formed architectures were also affected by the shape of their precursor crystal seeds. In the forming process (Fig. 3) of **BTN-6** microtubes, the crystallization is performed on the interface of the THF and hexane, which provides a limited factor as a soft template. Due to the poor solubility of **BTN-6** in hexane, the rate of crystallization at the interface of two phases is higher than that of diffusion of **BTN-6** from THF into hexane. The aggregates of **BTN-6** tend to stack along the *c*-axis due to



Fig. 3 Schematic representation of the self-assembly processes of **BTN-6**.

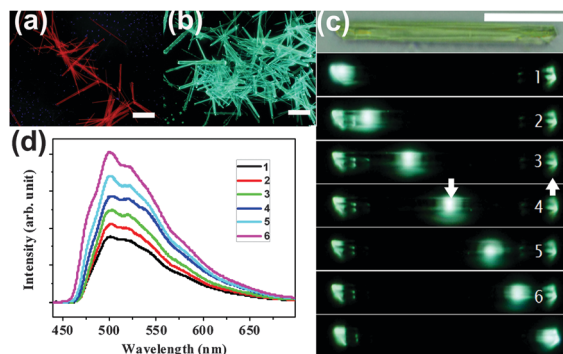


Fig. 4 PL images of microstructures of **BTN-6** (a) and **BTN-7** (b). Scale bars are 50 μm . (c) Microarea PL images obtained by exciting an identical microrod at different positions, down arrow (excited site) and up arrow (emitted tip). Scale bar is 20 μm . (d) Corresponding PL spectra in c.

the strong π - π interactions and hydrogen bonds. The tubular structure of the molecular crystal was easily formed along the growth direction of the template wall. The growth rates along the wall exceed greatly the growth in the middle of the template. Simultaneously, owing to the surface energy among different facets of the 1-D aggregation, the redissolving starts at the center of the high energy facet, and then continues toward the inside along the c -axis.^{16,17} Therefore, a perfect crystal tubule-like structure can be obtained. However, in the mixture of ethanol/THF, the growth rate and direction of the molecular crystal aggregates is the same in the soft template, due to the influence of the hydrogen bond interactions being weak; the 1-D rod-like structures were easily formed. The rate of crystallization at the interface of two phases is near to that of the diffusion of **BTN-6** THF solution into ethanol due to the good miscibility of THF and ethanol, which results in rod-like aggregation.¹⁶⁻¹⁸

Fluorescence microscopic images (Fig. 4) confirmed that the microstructures of ICT compounds were intense emitters. The results indicated that the prepared microrods of **BTN-6** exhibited strong red emission, while **BTN-7** exhibited green emission. Furthermore, the distance-dependent photoluminescence image of a single microrod of **BTN-7** was measured with a near-field scanning optical microscope. As shown in Fig. 4c, the corresponding spatially resolved PL spectra were detected by changing the excitation laser beam at different points. In this study, the intensity at the body excited site (I_{body}) and emitted tip (I_{tip}) were recorded and the optical loss coefficient (α) was calculated by a single exponential fitting.¹⁹ For **BTN-7**, the average evaluation of the waveguide loss coefficient α was determined to be 0.018 dB μm^{-1} and no obvious red-shift was observed with the increase of propagation distance. Here, the negligible reabsorption, smooth surface and distinctly flat end facets contributed to this excellent optical waveguide behavior. These results demonstrate that the as-prepared **BTN-7** microrods are potential excellent optical waveguide materials. The conductive properties of a single microrod were investigated tentatively with bottom-contact devices. The measurements were performed using a two-probe method under ambient conditions, and the collected current-voltage (I - V) curves (Fig. S7†) were nearly linear with a small contact barrier.

The electrical conductivity value of **BTN-6** was estimated to be $1.64 \times 10^{-5} \text{ S m}^{-1}$, showing the semiconducting character of this material.

In summary, two kinds of intramolecular charge-transfer molecules have been synthesized for studying the tuning of molecular aggregate structures by self-assembly technology. The resulting controllable aggregate structures of these intramolecular charge transfer compounds show highly uniform tubule, rod and cubic like architectures in large quantities and with high morphological and chemical purity. The fabricated **BTN-7** microrods exhibit outstanding optical waveguide properties with a waveguide efficiency α of 0.018 dB μm^{-1} and no obvious red-shift was observed. As a result, they could possess highly interesting potential applications in optical devices.

We thank the National Nature Science Foundation of China (201031006 and 90922017) and the National Basic Research 973 Program of China (2011CB932302 and 2012CD932900).

Notes and references

† Crystal data for **BTN-6**: $\text{C}_{34}\text{H}_{20}\text{N}_4\text{O}_2\text{S}$, $M_r = 548.60$, monoclinic, space group: $P2_1/n$, $a = 10.064(2)$, $b = 8.9812(18)$, $c = 28.804(6)$ \AA , $\alpha = 90$, $\beta = 97.80(3)$, $\gamma = 90^\circ$, $V = 2579.5(9)$ \AA^3 , $Z = 4$, $T = 173(2)$ K, $D_{\text{calcd}} = 1.413 \text{ mg m}^{-3}$, $R_1 = 0.0991$ ($I > 2\sigma(I)$), $R_w = 0.1908$ (all data), GOF = 1.143; **BTN-7**: $\text{C}_{34}\text{H}_{21}\text{N}_3\text{S}$, $M_r = 503.60$, monoclinic, space group: $P2_1/c$, $a = 9.0702(18)$, $b = 39.586(8)$, $c = 7.4369(15)$ \AA , $\alpha = 90$, $\beta = 106.217(3)$, $\gamma = 90^\circ$, $V = 2564.0(9)$ \AA^3 , $Z = 4$, $T = 173(2)$ K, $D_{\text{calcd}} = 1.305 \text{ mg m}^{-3}$, $R_1 = 0.0746$ ($I > 2\sigma(I)$), $R_w = 0.1501$ (all data), GOF = 1.199. CCDC-859087 for **BTN-6** and CCDC-859088 for **BTN-7**.

- Z. L. Wang, *Adv. Mater.*, 2003, **15**, 432.
- M. Law, L. E. Greene, C. J. Johnson, R. Saykally and P. Yang, *Nat. Mater.*, 2005, **4**, 455.
- H. Liu, Y. Li, L. Jiang, H. Luo, S. Xiao, H. Fang, H. Li, D. Zhu, D. Yu, J. Xu and B. Xiang, *J. Am. Chem. Soc.*, 2002, **124**, 13370.
- B.-K. An, S.-K. Kwon and S. Y. Park, *Angew. Chem., Int. Ed.*, 2007, **46**, 1978.
- H. Liu, J. Xu, Y. Li and Y. Li, *Acc. Chem. Res.*, 2010, **43**, 1496.
- S. Chen, Y. Li, W. Yang, N. Chen, H. Liu and Y. Li, *J. Phys. Chem. C*, 2010, **114**, 15109.
- A. B. Koren, M. D. Curtis, A. H. Francis and J. W. Kampf, *J. Am. Chem. Soc.*, 2003, **125**, 5040.
- Z. Xie, B. Yang, F. Li, G. Cheng, L. Liu, G. Yang, H. Xu, L. Ye, M. Hanif, S. Liu, D. Ma and Y. Ma, *J. Am. Chem. Soc.*, 2005, **127**, 14152.
- X. Feng, B. Tong, J. Shen, J. Shi, T. Han, L. Chen, J. Zhi, P. Lu, Y. Ma and Y. Dong, *J. Phys. Chem. B*, 2010, **114**, 16731.
- P. Anant, N. T. Lucas and J. Jacob, *Org. Lett.*, 2008, **10**, 5533.
- S. Kato, T. Matsumoto, T. Ishi, T. Thiemann, M. Shigeiwa, H. Gorohmaru, S. Maeda, Y. Yamashita and S. Mataka, *Chem. Commun.*, 2004, 2342.
- Y. Yu, Y. N. Hong, C. Feng, J. Z. Liu, J. W. Y. Lam, M. T. Faisal, K. M. Ng, K. Q. Luo and B. Z. Tang, *Sci. China, Ser. B: Chem.*, 2009, **52**, 15.
- J. Chen, C. C. W. Law, J. W. Y. Lam, Y. Dong, S. M. F. Lo, I. D. Williams, D. Zhu and B. Z. Tang, *Chem. Mater.*, 2003, **15**, 1535.
- K. Balakrishnan, A. Datar, T. Naddo, J. Huang, R. Oitker, M. Yen, J. Zhao and L. Zang, *J. Am. Chem. Soc.*, 2006, **128**, 7390.
- K. Balakrishnan, A. Datar, R. Oitker, H. Chen, J. Zuo and L. Zang, *J. Am. Chem. Soc.*, 2005, **127**, 10496.
- L. Zang, Y. Che and J. S. Moore, *Acc. Chem. Res.*, 2008, **41**, 1596.
- X. J. Zhang, X. H. Zhang, W. S. Shi, X. M. Meng, C. S. Lee and S. T. Lee, *Angew. Chem., Int. Ed.*, 2007, **46**, 1525.
- Y. S. Zhao, H. Fu, A. Peng, Y. Ma, Q. Liao and J. Yao, *Acc. Chem. Res.*, 2010, **43**, 409.
- C. J. Barrelet, A. B. Greytak and C. M. Lieber, *Nano Lett.*, 2004, **4**, 1981.